Erschienen in: Physical Review Letters ; 115 (2015), 26. - 263601
https://dx.doi.org/10.1103/PhysRevLett.115.263601

Paraxial Theory of Direct Electro-optic Sampling of the Quantum Vacuum

A. S. Moskalenko,* C. Riek, D. V. Seletskiy, G. Burkard, and A. Leitenstorfer
Department of Physics and Center for Applied Photonics, University of Konstanz, D 78457 Konstanz, Germany

Direct detection of vacuum fluctuations and analysis of subcycle quantum properties of the electric field are explored by a paraxial quantum theory of ultrafast electro optic sampling. The feasibility of such experiments is demonstrated by realistic calculations adopting a thin ZnTe electro optic crystal and stable few femtosecond laser pulses. We show that nonlinear mixing of a short near infrared probe pulse with the multiterahertz vacuum field leads to an increase of the signal variance with respect to the shot noise level. The vacuum contribution increases significantly for appropriate length of the nonlinear crystal, short pulse duration, tight focusing, and a sufficiently large number of photons per probe pulse. If the vacuum input is squeezed, the signal variance depends on the probe delay. Temporal positions with a noise level below the pure vacuum may be traced with subcycle resolution.

Finite fluctuation amplitudes in the ground state of empty space represent the ultimate hallmark of the quantum nature of the electromagnetic radiation field. These vacuum fluctuations manifest themselves indirectly in a number of phenomena that are accessible to spectroscopy such as the spontaneous decay of excited atomic states as well as the Lamb shift [1] in atoms [2] and in quantum-mechanical electric circuits [3]. Access to the quantum aspects of electromagnetic radiation is provided by the analysis of photon correlation [4,5] or homodyning [6–11] measurements. However, these approaches require amplification of the quantum field under study to finite intensity and information is typically averaged over multiple optical cycles.

On the other side, precise determination of a voltage or electric field amplitude as a function of time represents a fundamental task in science and engineering. Optical techniques have to be applied when detecting electric fields oscillating in the terahertz (THz) range and above. Those approaches involve probing with ultrashort laser pulses of a temporal duration on the order of half an oscillation period at the highest frequencies under study. Far-infrared electric transients [12,13] may be characterized by photoconductive switching [14]. Electro-optic sampling in free space [15–17] allows field-resolved detection at high sensitivity in the entire far- and midinfrared spectral range [18,19]. Direct studies of the complex-valued susceptibilities of materials and the elementary dynamics in condensed matter are performed with these methods [20,21]. The time integral of near-infrared to visible electric-field wave packets is accessible with attosecond streaking [22]. So far, all those techniques were restricted to the classical field amplitude. Very recently, direct access to the vacuum fluctuations of the multi-THz electric field has been established experimentally [23].

In this Letter, we demonstrate theoretically that the quantum properties of light may be accessed directly in the time domain, i.e., with subcycle temporal resolution. Our considerations are based on the realistic example of electro-optic detection with zinc-blende-type materials [24]. Even vacuum fluctuations may be sampled without amplification by broadband probing of electric field amplitudes in the multi-THz region with few-femtosecond laser pulses of moderate energy content.

We consider the geometry sketched in Fig. 1. An ultrashort near-infrared (NIR) wave packet with electric field $\mathbf{E}_p$ propagates along the [110] axis of an electro-optic crystal (EOX) [24,25]. Its wave vector $\mathbf{k}_\omega$ is perpendicular to the z axis $\mathbf{e}_z$ of the EOX. We select $\mathbf{E}_p \| \mathbf{e}_z$ [26]. In this configuration, the second-order nonlinear mixing of $\mathbf{E}_p(t)$

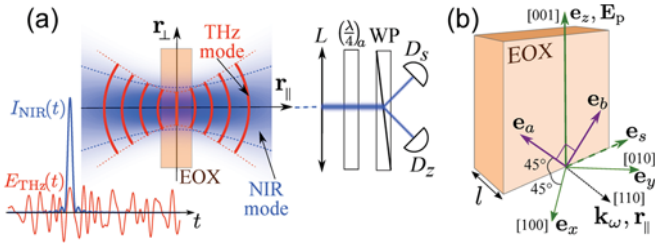

FIG. 1 (color online). Setup and geometry for free space electro optic sampling. (a) The incoming near infrared (NIR) probe and multi THz signal fields mix in the electro optic crystal (EOX). The NIR (blue) spatial mode amplitude is depicted by the contour plot, whereas a THz (red) spatial mode is indicated by wave fronts. Bottom left corner: temporal profiles of the NIR intensity envelope $I_{\mathrm{NIR}}(t)$ and a representative multi THz vac uum field $E_{\mathrm{THz}}(t)$. After collimating with a lens (L), the modified NIR field is analyzed using a quarter wave plate $(\lambda/4)_a$, a Wollaston prism (WP), and balanced detectors (D_s, D_z) measuring the difference in photon flux of the split components. (b) Spatial directions determining the electro optic effect in a zinc blende type EOX and the following ellipsometry analysis.

with an incident THz field $\hat{\mathbf{E}}_{\mathrm{THz}}(t)$ induces nonlinear polarization in the EOX plane with the components [26]

$$\hat{P}_s^{(2)}(t) = -\epsilon_0 d \hat{E}_{\mathrm{THz},s}(t) E_p(t), \qquad \hat{P}_z^{(2)}(t) = 0. \tag{1}$$

ϵ_0 is the vacuum permittivity. The coupling constant $d = -n^4 r_{41}$ can be determined from the electro-optic coefficient r_{41} and refractive index (RI) n at the center frequency ω_c of $\mathbf{E}_p$ [32–34]. In general, both fields $\hat{E}_{\mathrm{THz}} \equiv \hat{E}_{\mathrm{THz},s}$ and $\hat{P}_s^{(2)}$ in Eq. (1) are quantized, whereas $E_p = E_{p,z} = \langle \hat{E}_{p,z} \rangle$ denotes the classical part of the probe field. We neglect the effect of quantum mechanical fluctuations of the probe field on $\hat{\mathbf{P}}^{(2)}$, assuming a sufficiently large E_p.

The nonlinear polarization $\hat{\mathbf{P}}^{(2)}$ represents a source in the inhomogeneous wave equation describing the evolution of the electric field $\hat{\mathbf{E}}$ in the EOX. The fields $\hat{\mathbf{F}} = \hat{\mathbf{E}}, \hat{\mathbf{P}}^{(2)}$ propagating in the forward direction $r_\parallel$ (see Fig. 1) can be decomposed as $\hat{\mathbf{F}}(\mathbf{r}, t) = \int_\infty^\infty d\omega \hat{\mathbf{F}}(\mathbf{r}; \omega) e^{i(k_\omega r_\parallel \ \omega t)}$, where $k_\omega = \omega n_\omega / c_0$. c_0 and n_ω are the velocity of light and the frequency-dependent RI of the EOX, respectively. Using the paraxial approximation [35,36], the inhomogeneous wave equation reads

$$\left[\Delta_\perp + 2ik_\omega \frac{\partial}{\partial r_\parallel} \right] \hat{\mathbf{E}}(\mathbf{r}; \omega) = -\frac{\omega^2}{\epsilon_0 c_0^2} \hat{\mathbf{P}}^{(2)}(\mathbf{r}; \omega), \tag{2}$$

where $\mathbf{r}_\perp = (r_s, r_z)$ and $\Delta_\perp = (\partial^2/\partial r_s^2) + (\partial^2/\partial r_z^2)$. From Eq. (1) we obtain $\hat{P}_s^{(2)}(\mathbf{r};\omega) = -\epsilon_0 d \int_\infty^\infty d\Omega \hat{E}_{\mathrm{THz}}(\mathbf{r};\Omega) \times E_p(\mathbf{r};\omega-\Omega) e^{i(k_\Omega + k_{\omega-\Omega} \ k_\omega) r_\parallel}$. The electric field of the probe beam provides a solution of the homogeneous part of Eq. (2) which can be expanded into Laguerre-Gaussian (LG) modes [37,38] (see Ref. [26]). We adopt a probe pulse train with a fundamental Gaussian transverse mode of amplitude $\alpha_p(\omega)$:

$$E_p(\mathbf{r}; \omega) = \alpha_p(\omega) \mathrm{LG}_{00}(\mathbf{r}_\perp, r_\parallel; k_\omega). \tag{3}$$

A length l of the EOX much shorter than the Rayleigh range of a beam at the relevant THz frequencies Ω with waist size w_0 is assumed, i.e., $l \ll k_\Omega w_0^2/2$.

The EOX is located at the beam waist $r_\parallel = 0$. It has antireflection coating on its surfaces. Denoting $\hat{\mathbf{F}}(\mathbf{r}_\perp; \omega) \equiv \hat{\mathbf{F}}(\mathbf{r}_\perp, r_\parallel = 0; \omega)$ we find that at the exit from the EOX, $r_\parallel = l/2$, the total electric field in the (110) plane is given by

$$\hat{\mathbf{E}}'(\mathcal{Y}) = E_p(\mathcal{Y}) \mathbf{e}_z + \hat{E}^{(2)}(\mathcal{Y}) \mathbf{e}_s + \delta \hat{\mathbf{E}}'(\mathcal{Y}), \tag{4}$$

where $\mathcal{Y} \equiv \{\mathbf{r}_\perp; \omega\}$. $\delta \hat{\mathbf{E}}'(\mathcal{Y}) = \hat{\mathbf{E}}_p(\mathcal{Y}) - E_p(\mathcal{Y}) \mathbf{e}_z$ denotes the contribution of the vacuum field at the probe frequency ω in the vacuum picture [39]. The correction to the probe field generated in the EOX is evaluated as

$$\hat{E}^{(2)}(\mathbf{r}_\perp; \omega) = \int_\infty^\infty d\Omega \hat{E}_{\mathrm{THz}}(\mathbf{r}_\perp; \Omega) E_p(\mathbf{r}_\perp; \omega - \Omega) \zeta_{\omega,\Omega}, \tag{5}$$

where the factor $\zeta_{\omega,\Omega} = -id(l\omega/2c_0 n) \mathrm{sinc}[(l\Omega/2c_0) \times (n_\Omega - n_g)]$ determines phase matching. Here $\mathrm{sinc}(x) \equiv \sin(x)/x$, n_Ω is the RI at Ω, whereas n and n_g are the RI and the group RI $c_0 \partial k_\omega / \partial \omega$ at $\omega = \omega_c$, respectively. Going beyond Ref. [17] where an expression similar to Eq. (5) was derived for the case of plane waves in order to establish a classical theory of electro-optic sampling, Eqs. (4) and (5) include the transverse spatial dependence of the fields, the quantized form of the signal, as well as the contribution of quantum fluctuations at the probe frequencies. These points are crucial for our further analysis.

From Eq. (4) we see that nonlinear mixing of the probe and THz components generates a new field which is polarized perpendicularly to the probe and propagates into the same direction. For the analysis of the polarization state of the modified probe, we consider the field components in the coordinate frame $\mathbf{e}_{b}^{a} = (\mathbf{e}_z \mp \mathbf{e}_s)/\sqrt{2}$ rotated by 45° with respect to the $\mathbf{e}_{z,s}$ frame [Fig. 1(b)], $\hat{E}_{b}^{\prime a}(\mathcal{Y}) = E_p(\mathcal{Y})[1 \pm i\hat{\phi}(\mathcal{Y})]/\sqrt{2} + \delta \hat{E}_{b}^{\prime a}(\mathcal{Y})$. Here $\hat{\phi}(\mathcal{Y}) = i\hat{E}^{(2)}(\mathcal{Y})/E_p(\mathcal{Y})$ must be small within the frequency bandwidth of the probe.

The ellipsometry scheme used in typical experiments is explained in Fig. 1(a). We consider its effects at the exit surface of the EOX. This simplification is justified when all probe photons are detected without spatial filtering. The quarter-wave plate shifts the phase of the a component of the field by $\pi/2$: $\hat{E}_a''(\mathcal{Y}) = i\hat{E}_a'(\mathcal{Y})$, $\hat{E}_b''(\mathcal{Y}) = \hat{E}_b'(\mathcal{Y})$. Subsequently, the Wollaston prism splits the electric field into its z and s components:

$$\hat{E}_{s}^{\prime\prime z}(\mathcal{Y}) = \frac{e^{\pm i(\pi/4)} E_p(\mathcal{Y})}{\sqrt{2}} [1 \mp \hat{\phi}(\mathcal{Y})] + \delta \hat{E}_{s}^{\prime\prime z}(\mathcal{Y}). \tag{6}$$

Finally, the photon numbers in both components are detected and subtracted. The photon number operator for the polarization $\alpha = z, s$ reads [40]

$$\hat{\mathcal{N}}_\alpha = C \int_0^\infty d\omega \frac{\eta(\omega)}{\hbar\omega} \int d^2 r_\perp \hat{E}_\alpha''^\dagger(\mathbf{r}_\perp; \omega) \hat{E}_\alpha''(\mathbf{r}_\perp; \omega), \tag{7}$$

where $C = 4\pi c_0 n \epsilon_0$, the dagger denotes Hermitian conjugation and the spatial integral covers the entire transverse profile of the probe beam. The frequency-dependent quantum efficiency of the photodetector $\eta(\omega) \approx 1$ over the detected frequency range but vanishes quickly for $\omega \to 0$.

Inserting Eq. (6) into Eq. (7) and neglecting the second-order terms in $\delta \hat{\mathbf{E}}''$ as well as the mixed terms depending linearly both on $\delta \hat{\mathbf{E}}''$ and on $\hat{E}_{\mathrm{THz}}$ (contained in $\hat{\phi}$) [42], the total detected quantum signal becomes

$$\hat{\mathcal{S}} \equiv \hat{\mathcal{N}}_s - \hat{\mathcal{N}}_z = \hat{\mathcal{S}}_{\mathrm{EO}} + \hat{\mathcal{S}}_{\mathrm{SN}}. \quad (8)$$

Here, the electro-optic signal (EOS) $\hat{\mathcal{S}}_{\mathrm{EO}}$ is

$$\hat{\mathcal{S}}_{\mathrm{EO}} = C \int d^2 r_\perp \int_0^\infty d\omega \frac{\eta(\omega)}{\hbar\omega} |E_p(\boldsymbol{\mathcal{Y}})|^2 [\hat{\phi}(\boldsymbol{\mathcal{Y}}) + \mathrm{H.c.}] \quad (9)$$

and the shot noise (SN) contribution $\hat{\mathcal{S}}_{\mathrm{SN}}$ reads $\hat{\mathcal{S}}_{\mathrm{SN}} = C \int d^2 r_\perp \int_0^\infty d\omega [\eta(\omega)/\hbar\omega][E_p^*(\boldsymbol{\mathcal{Y}}) \delta\hat{E}''_+(\boldsymbol{\mathcal{Y}}) + \mathrm{H.c.}]$. H.c. denotes the Hermitian conjugate and $\delta\hat{E}''_+(\boldsymbol{\mathcal{Y}}) = e^{i\pi/4}[\delta\hat{E}''_s(\boldsymbol{\mathcal{Y}}) + i\delta\hat{E}''_z(\boldsymbol{\mathcal{Y}})]/\sqrt{2}$ is the circular component of the vacuum contribution of the probe field [43]. Summing up the signals from both detectors, the expectation value of the number of detected photons per probe pulse $N = \langle \hat{\mathcal{N}}_s + \hat{\mathcal{N}}_z \rangle = (4\pi c_0 n \epsilon_0/\hbar) \int_0^\infty d\omega [\eta(\omega)/\omega] \times |\alpha_p(\omega)|^2$ results.

Using Eqs. (3) and (5) in Eq. (9), we obtain

$$\hat{\mathcal{S}}_{\mathrm{EO}} = \frac{dlN\omega_p}{c_0 n} \int d^2 r_\perp g_{00}^2(\mathbf{r}_\perp) \int_\infty^\infty d\Omega \hat{E}_{\mathrm{THz}}(\mathbf{r}_\perp; \Omega) R(\Omega). \quad (10)$$

$g_{00}(\mathbf{r}_\perp) \equiv \mathrm{LG}_{00}(\mathbf{r}_\perp, r_\parallel = 0; k_\omega) = \sqrt{2/\pi} w_0^{-1} \exp(-r_\perp^2/w_0^2)$ is a normalized Gaussian independent of ω and $\omega_p = \int_0^\infty d\omega \eta(\omega) |\alpha_p(\omega)|^2 / \int_0^\infty d\omega [\eta(\omega)/\omega] |\alpha_p(\omega)|^2$ is the average detected frequency. We have introduced the response function $R(\Omega) = \mathrm{sinc}[(l\Omega/2c_0)(n_\Omega - n_g)] f(\Omega)$ with the normalized Hermitian spectral autocorrelation function $f(\Omega) = [f_+^*(\Omega) + f\ (\Omega)]/2$, where $f_\pm(\Omega) = \int_0^\infty d\omega \eta(\omega) \alpha_p^*(\omega) \alpha_p(\omega \pm \Omega) / \int_0^\infty d\omega \eta(\omega) |\alpha_p(\omega)|^2$.

Within the paraxial quantization [38], $\hat{E}_{\mathrm{THz}}(\mathbf{r}_\perp; \Omega)$ in Eq. (10) is given by [26]

$$\hat{E}_{\mathrm{THz}}(\mathbf{r}_\perp; \Omega) = -i \sum_{l,p} \sqrt{\frac{\hbar\Omega}{4\pi\epsilon_0 c_0 n_\Omega}} \hat{a}_{s,l,p}(\Omega) g'_{lp}(\mathbf{r}_\perp) \quad (11)$$

for $\Omega > 0$, $\hat{E}_{\mathrm{THz}}(\mathbf{r}_\perp; \Omega < 0) = \hat{E}_{\mathrm{THz}}^\dagger(\mathbf{r}_\perp; -\Omega)$. Here, $\hat{a}_{s,l,p}(\Omega)$ annihilates a photon with frequency Ω, orbital quantum numbers l, p, and polarization $\mathbf{e}_s$. We have introduced the transverse mode functions $g'_{lp}(\mathbf{r}_\perp) \equiv \mathrm{LG}_{lp}(\mathbf{r}_\perp, r_\parallel = 0; k_\Omega)$. In contrast to the probe beam, the waist size $w_0{}'$ characterizing these mode functions is a free parameter of the expansion (11). Inserting Eq. (11) into Eq. (10) and selecting $w_0{}' = w_0/\sqrt{2}$, we can evaluate the spatial integral using $\int d^2 r_\perp g_{00}^2(\mathbf{r}_\perp) g'_{lp}(\mathbf{r}_\perp) = (1/\sqrt{\pi} w_0) \delta_{l,0} \delta_{p,0}$. Then we obtain from Eq. (10)

$$\hat{\mathcal{S}}_{\mathrm{EO}} = -i\sqrt{B} \int_0^\infty d\Omega \sqrt{\frac{\Omega}{n_\Omega}} [\hat{a}_{s,0,0}(\Omega) R(\Omega) - \mathrm{H.c.}], \quad (12)$$

where $B = (d^2 l^2 N^2 \omega_p^2 \hbar)/(4\pi^2 \epsilon_0 c_0^3 n^2 w_0^2)$.

As an input, we now consider a THz quantum field with no coherent (classical) contribution: $\langle \hat{E}_{\mathrm{THz}} \rangle = 0$, e.g., a bare multi-THz vacuum. Then $\langle \hat{\mathcal{S}} \rangle = 0$ since $\langle \hat{\mathcal{S}}_{\mathrm{SN}} \rangle = 0$ and $\hat{\phi}$ in Eq. (9) depends linearly on $\hat{E}_{\mathrm{THz}}$, thus also $\langle \hat{\mathcal{S}}_{\mathrm{EO}} \rangle = 0$. However, the variance of the signal does not vanish. If the range of detected THz frequencies, determined by $R(\Omega)$, does not overlap with the frequency content of the probe beam, the signal variance $\langle \hat{\mathcal{S}}^2 \rangle - \langle \hat{\mathcal{S}} \rangle^2 = \langle \hat{\mathcal{S}}^2 \rangle$ can be written as $\langle \hat{\mathcal{S}}^2 \rangle = \langle \hat{\mathcal{S}}_{\mathrm{EO}}^2 \rangle + \langle \hat{\mathcal{S}}_{\mathrm{SN}}^2 \rangle$. Calculating the SN contribution using the paraxial quantization [38], we obtain the expected result $\langle \hat{\mathcal{S}}_{\mathrm{SN}}^2 \rangle = N$.

Evaluating $\langle \hat{\mathcal{S}}_{\mathrm{EO}}^2 \rangle$ for the multi-THz vacuum yields

$$\langle \hat{\mathcal{S}}_{\mathrm{EO}}^2 \rangle = N^2 \left(n^3 \frac{l\omega_p}{c_0} r_{41} \right)^2 \frac{\hbar \int_0^\infty d\Omega \Omega (n/n_\Omega) |R(\Omega)|^2}{4\pi^2 \epsilon_0 c_0 n w_0^2}, \quad (13)$$

where we have used $\langle \hat{a}_{s,0,0}(\Omega) \hat{a}_{s,0,0}^\dagger(\Omega') \rangle = \delta(\Omega - \Omega')$. Note that the expectation values of all other possible quadratic combinations of $\hat{a}_{s,0,0}^\dagger$ and $\hat{a}_{s,0,0}$ vanish. The first two factors on the right-hand side of Eq. (13) determine the sampling efficiency. The fundamental physics is contained in the third factor representing the variance of the multi-terahertz vacuum field $(\Delta E)^2 = \hbar/(\epsilon_0 \Delta x \Delta y \Delta z \Delta t)$. The transverse area $\Delta x \Delta y$ is set by the cross section of the sampling mode which is proportional to w_0^2. The ratio of c_0 to the integral containing the response function $R(\Omega)$ determines the longitudinal cross-sectional area. It corresponds to the effective spatial length Δz times the temporal duration Δt of the sampling pulse which become modified by the phase-matching conditions and renormalized due to the refractive index n_Ω inside the EOX. Consequently, $\langle \mathcal{S}_{\mathrm{EO}}^2 \rangle$ may be modulated in an experiment by lateral or transverse expansion of the four-dimensional space-time volume over which the probe pulse averages while keeping $\langle \mathcal{S}_{\mathrm{SN}}^2 \rangle$ exactly constant [23].

To illustrate the results, we assume the following realistic specifications of the sampling few-femtosecond NIR laser pulse: center frequency 255 THz, spectral bandwidth 150 THz with rectangular spectral shape and flat phase, leading to $\omega_p = 247$ THz, and waist size $w_0 = 3$ μm [44]. We consider a $l = 7$ μm thick ZnTe EOX with $r_{41} = 4$ pm/V [45,46], $n = 2.76$, $n_g = 2.9$, and n_Ω varying only slightly (from 2.55 to 2.59) for the relevant THz frequencies [26]. The resulting integrand function entering Eq. (13) is shown in Fig. 2(a) (for details, see Ref. [26]). Diffraction effects are taken into account by excluding wavelengths λ with $\lambda/(2n_\Omega) > w_0$.

Based on this input, we calculate the dependence of the rms value of the signal $\Delta\mathcal{S} = \langle \hat{\mathcal{S}}^2 \rangle^{1/2}$ on the average number N of photons in the sampling NIR pulse, as shown in Fig. 2(b) on a double-logarithmic scale. Above a certain N, the EOS contribution of the multi-THz vacuum changes the typical SN scaling. The relative increase of the rms value of the signal with respect to the SN level, $(\Delta\mathcal{S} - \Delta\mathcal{S}_{\mathrm{SN}})/\Delta\mathcal{S}_{\mathrm{SN}}$, is depicted in Fig. 2(c) for moderate N and with linear scaling. For even higher N, the vacuum

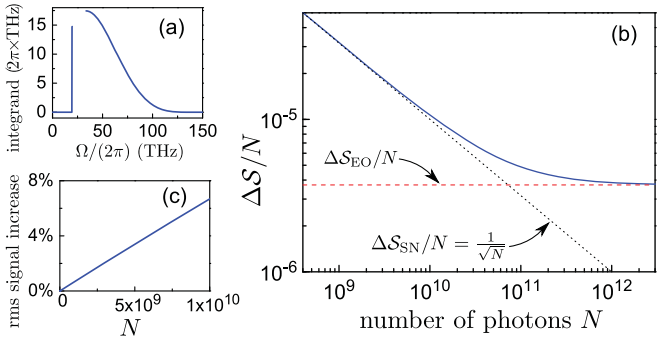

FIG. 2 (color online). (a) Calculated integrand function $\Omega(n/n_\Omega)|R(\Omega)|^2$ entering Eq. (13). (b) Double logarithmic plot of the ratio $\Delta\mathcal{S}/N$ in dependence on N. The black dotted (red dashed) line shows the bare SN (multi THz vacuum) contribu tion. (c) Increase of $(\Delta\mathcal{S}-\Delta\mathcal{S}_{\rm SN})/\Delta\mathcal{S}_{\rm SN}$ with N. Parameters are defined in the main text.

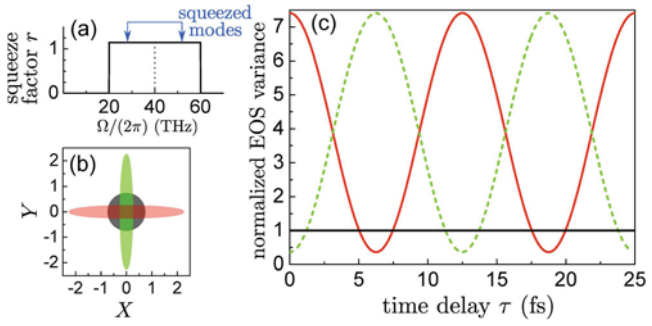

FIG. 3 (color online). (a) Frequency dependence of the squeeze factor r. Squeezing correlates Ω and $2\Omega_c-\Omega$ modes (as indicated by arrows). (b) Error contour in the complex amplitude plane for PV (gray circle) and SV with $\theta=0$ ($\theta=\pi$) [red (green) ellipse with reduced uncertainty in the phase (amplitude) quadrature Y (X)]. (c) Normalized (with respect to the constant PV level, solid black line) EOS variance in dependence on the time delay τ of the probe NIR pulse for SV with $\theta=0$ ($\theta=\pi$) [solid red line (dashed green line)].

contribution starts to dominate so that the dependence saturates to the constant EOS level [Fig. 2(b)]. Subtracting the SN contribution from the total signal variance, the bare EOS variance induced by the sampled quantum field can be analyzed.

To elaborate on this point, we apply our theory to a multi-THz vacuum which is squeezed in an interval around a center frequency Ω_c. The corresponding state of light is generated by the continuum squeezing operator [47–49] $\exp\{\frac{1}{2}\int_0^{2\Omega_c} d\Omega\sum_{\alpha lp}[\xi_\Omega^*\hat{a}_{\alpha,l,p}(2\Omega_c-\Omega)\hat{a}_{\alpha,l,p}(\Omega)-\text{H.c.}]\}$ acting on the multi-THz pure vacuum (PV) state considered above. The frequency-dependent squeezing parameter ξ_Ω satisfies the condition $\xi_\Omega=\xi_{2\Omega_c\ \Omega}$. We assume that all spatial and polarization modes are squeezed equally. In this case, the EOS can be obtained from Eq. (12) transforming $\hat{a}_{s,0,0}(\Omega)\to\hat{a}_{s,0,0}(\Omega)\cosh r_\Omega-\hat{a}^\dagger_{s,0,0}(2\Omega_c-\Omega)e^{i\theta_\Omega}\sinh r_\Omega$ [47–49] and working in the vacuum picture. The expectation value of the signal remains zero. Evaluation of the EOS variance for the squeezed vacuum (SV), $\langle\hat{\mathcal{S}}^2_{\rm EO}\rangle_{\rm SV}(\tau)$, is analogous to the PV case. However, the SV EOS variance depends on the time delay τ of the NIR probe pulse leading to the transformation $R(\Omega)\to R(\Omega)e^{\ i\Omega\tau}$ of the response function. This fact was unimportant for handling the PV [cf. Eq. (13)]. For a probe pulse symmetric with respect to $t=\tau$, i.e., $E_p(t-\tau)=E_p(\tau-t)$, we find $R(\Omega)=R_0(\Omega)e^{\ i\Omega\tau}$, where $R_0(\Omega)$ is real-valued.

For our illustration, we assume constant squeezing with $\xi_\Omega\equiv\xi=re^{i\theta}$ in the frequency range $[\Omega_1,\Omega_2]$ with $\Omega_c=(\Omega_1+\Omega_2)/2$, where $r=|\xi|$ is the squeeze factor [50,51] and $\theta=\text{Arg}(\xi)$ is the squeezing phase [48]. No squeezing occurs outside this range. In particular, we use $\Omega_c/(2\pi)=40$ THz, $\Omega_2-\Omega_1=\Omega_c$ and $\sinh r=2$ [see Fig. 3(a)]. Generalized quadrature operators [47] $\hat{X}_\lambda=[1/\sqrt{2}(\Omega_2-\Omega_1)]\int_{\Omega_1}^{\Omega_2}d\Omega[\hat{a}_{s,0,0}(\Omega)e^{\ i\lambda}+\text{H.c.}]$, with $\hat{X}=\hat{X}_0$ and $\hat{Y}=\hat{X}_{\pi/2}$, normalized so that $[\hat{X},\hat{Y}]=i$ are introduced. The error contours for PV as well as for the SV as described above and two different squeezing phases, $\theta=0$ and $\theta=\pi$, are featured in Fig. 3(b). The dependence of the normalized EOS variance $\langle\hat{\mathcal{S}}^2_{\rm EO}\rangle_{\rm SV}(\tau)/\langle\hat{\mathcal{S}}^2_{\rm EO}\rangle$, where $\langle\hat{\mathcal{S}}^2_{\rm EO}\rangle$ is given by Eq. (13), on the time delay τ is shown in Fig. 3(c) for the same states as in Fig. 3(b) and sampling parameters used for the PV case. For specific delay times, the EOS variance of the multi-THz SV is by 64% lower than the unsqueezed value of the PV state (for details, see Ref. [26]).

We emphasize the cardinal difference between our findings and similar-looking results obtained in the context of homodyning [52,53]. In homodyning experiments, the signal is determined by the temporal overlap integral of the *complex amplitudes* of the electric fields of an input state and a local oscillator; i.e., the information is typically averaged over multiple oscillation cycles of light. In contrast, electro-optic sampling provides a true subcycle resolution of the probed multi-THz *electric field*. Moreover, registration of photons is transferred into the NIR, circumventing the lack of efficient single-photon detectors in the multi-THz frequency range. Most importantly, the multi-THz quantum field may be studied without the necessity to reduce or amplify its photon content—even if it remains in its ground state. For a detailed discussion, see Ref. [26].

In conclusion, we theoretically clarify the contribution of the quantum fluctuations of the multi-THz vacuum electric field to the signal in ultrabroadband electro-optic sampling by differentiating it from the trivial shot noise of the high-frequency gating pulse. The crucial aspects are a strong localization of the sampling beam in space and time as it passes the nonlinear crystal, a large second-order nonlinear coefficient and proper phase matching that might be further optimized selecting an even more appropriate material than the thin piece of ZnTe we have considered as an example [23]. For a multi-THz squeezed vacuum, the possibility to trace the

oscillations of the EOS variance with the time delay of the probe pulse is predicted. Positions occur where the noise remains significantly below the level of unsqueezed vacuum. The same formalism can be applied for the analysis of more complex quantum fields in a time-resolved and nondestructive manner. Experimental implementation of these ideas might open up a new chapter of quantum optics operating predominantly in the time domain and with subcycle access to the quantum state of electromagnetic radiation.

Funding by the ERC (Advanced Grant No. 290876 "UltraPhase") and DFG (SFB 767) is gratefully acknowledged. We thank M. Kira for helpful discussions.

*andrey.moskalenko@uni konstanz.de

[1] J. J. Sakurai, *Advanced Quantum Mechanics* (Addison Wesley, Reading, 1967).
[2] W. E. Lamb and R. C. Retherford, Phys. Rev. **72**, 241 (1947).
[3] A. Fragner, M. Goppl, J. M. Fink, M. Baur, R. Bianchetti, P. J. Leek, A. Blais, and A. Wallraff, Science **322**, 1357 (2008).
[4] R. Hanbury Brown and R. Q. Twiss, Nature (London) **177**, 27 (1956).
[5] H. J. Kimble, M. Dagenais, and L. Mandel, Phys. Rev. Lett. **39**, 691 (1977).
[6] J. Shapiro, H. P. Yuen, and A. Mata, IEEE Trans. Inf. Theory **25**, 179 (1979).
[7] L. Mandel, Phys. Rev. Lett. **49**, 136 (1982).
[8] R. E. Slusher, L. W. Hollberg, B. Yurke, J. C. Mertz, and J. F. Valley, Phys. Rev. Lett. **55**, 2409 (1985).
[9] D. T. Smithey, M. Beck, M. G. Raymer, and A. Faridani, Phys. Rev. Lett. **70**, 1244 (1993).
[10] G. Breitenbach, S. Schiller, and J. Mlynek, Nature (London) **387**, 471 (1997).
[11] C. Silberhorn, Contemp. Phys. **48**, 143 (2007).
[12] D. H. Auston, K. P. Cheung, and P. R. Smith, Appl. Phys. Lett. **45**, 284 (1984).
[13] Ch. Fattinger and D. Grischkowsky, Appl. Phys. Lett. **54**, 490 (1989).
[14] D. H. Auston, Appl. Phys. Lett. **26**, 101 (1975).
[15] Q. Wu and X. Zhang, Appl. Phys. Lett. **67**, 3523 (1995).
[16] A. Nahata, A. S. Weling, and T. F. Heinz, Appl. Phys. Lett. **69**, 2321 (1996).
[17] G. Gallot and D. Grischkowsky, J. Opt. Soc. Am. B **16**, 1204 (1999).
[18] K. Liu, J. Xu, and X. C. Zhang, Appl. Phys. Lett. **85**, 863 (2004).
[19] C. Kübler, R. Huber, S. Tübel, and A. Leitenstorfer, Appl. Phys. Lett. **85**, 3360 (2004).
[20] D. N. Basov, R. D. Averitt, D. van der Marel, M. Dressel, and K. Haule, Rev. Mod. Phys. **83**, 471 (2011).
[21] R. Ulbricht, E. Hendry, J. Shan, T. F. Heinz, and M. Bonn, Rev. Mod. Phys. **83**, 543 (2011).
[22] E. Goulielmakis, M. Uiberacker, R. Kienberger, A. Baltuska, V. Yakovlev, A. Scrinzi, T. Westerwalbesloh, U. Kleineberg, U. Heinzmann, M. Drescher, and F. Krausz, Science **305**, 1267 (2004).
[23] C. Riek, D. V. Seletskiy, A. S. Moskalenko, J. F. Schmidt, P. Krauspe, S. Eckart, S. Eggert, G. Burkard, and A. Leitenstorfer, Science **350**, 420 (2015).
[24] P. C. M. Planken, H. K. Nienhuys, H. J. Bakker, and T. Wenckebach, J. Opt. Soc. Am. B **18**, 313 (2001).
[25] S. Namba, J. Opt. Soc. Am. **51**, 76 (1961).
[26] See Supplemental Material at http://link.aps.org/supplemental/10.1103/PhysRevLett.115.263601, which includes Refs. [27 31], for details.
[27] M. Abramowitz and I. Stegun, *Handbook of Mathematical Functions: With Formulas, Graphs, and Mathematical Tables* (Dover, New York, 2012).
[28] R. Loudon, *The Quantum Theory of Light* (Oxford University Press, New York, 2000).
[29] W. Sellmeier, Ann. Phys. (Berlin) **219**, 272 (1871).
[30] D. T. F. Marple, J. Appl. Phys. **35**, 539 (1964).
[31] A. I. Lvovsky and M. G. Raymer, Rev. Mod. Phys. **81**, 299 (2009).
[32] G. New, *Introduction to Nonlinear Optics* (Cambridge University Press, New York, 2011).
[33] P. E. Powers, *Fundamentals of Nonlinear Optics* (Taylor & Francis, Boca Raton, 2011).
[34] A. Yariv, *Quantum Electronics* (John Wiley & Sons, New York, 1989).
[35] R. W. Boyd, *Nonlinear Optics*, 3rd ed. (Academic Press, Burlington, 2008).
[36] Y. R. Shen, *Principles of Nonlinear Optics* (Wiley Interscience, New York, 1984).
[37] L. Allen, M. W. Beijersbergen, R. J. C. Spreeuw, and J. P. Woerdman, Phys. Rev. A **45**, 8185 (1992).
[38] G. F. Calvo, A. Picón, and E. Bagan, Phys. Rev. A **73**, 013805 (2006).
[39] P. Knight and L. Allen, *Concepts of Quantum Optics* (Pergamon Press, Oxford, 1983).
[40] See Ref. [41] for a case with a simpler transverse mode structure.
[41] M. G. Raymer, J. Cooper, H. J. Carmichael, M. Beck, and D. T. Smithey, J. Opt. Soc. Am. B **12**, 1801 (1995).
[42] The mixed terms were also neglected already in Eq. (1). The second order terms in $\delta\hat{E}''$ ($\delta\hat{E}_z''^{\dagger}\delta\hat{E}_z''$ and $\delta\hat{E}_s''^{\dagger}\delta\hat{E}_s''$) do not contribute to the expectation value of the signal, neither to its variance or any higher moments.
[43] The phase shift is of no physical importance for the vacuum field contribution.
[44] D. Brida, G. Krauss, A. Sell, and A. Leitenstorfer, Laser Photonics Rev. **8**, 409 (2014).
[45] A. Cingolani, M. Ferrara, and M. Lugarà, Solid State Commun. **38**, 819 (1981).
[46] A. Leitenstorfer, S. Hunsche, J. Shah, M. C. Nuss, and W. H. Knox, Appl. Phys. Lett. **74**, 1516 (1999).
[47] S. Barnett and P. Radmore, *Methods in Theoretical Quantum Optics*, Oxford Series in Optical and Imaging Sciences (Oxford University Press, New York, 2002).
[48] W. Vogel and D. Welsch, *Quantum Optics* (Wiley, Weinheim, 2006).
[49] K. J. Blow, R. Loudon, S. J. D. Phoenix, and T. J. Shepherd, Phys. Rev. A **42**, 4102 (1990).
[50] C. M. Caves, Phys. Rev. D **23**, 1693 (1981).
[51] D. Walls and G. Milburn, *Quantum Optics* (Springer, Berlin, 2008).
[52] M. E. Anderson, D. F. McAlister, M. G. Raymer, and M. C. Gupta, J. Opt. Soc. Am. B **14**, 3180 (1997).
[53] R. E. Slusher, P. Grangier, A. LaPorta, B. Yurke, and M. J. Potasek, Phys. Rev. Lett. **59**, 2566 (1987).